5.5–7.5 MeV Proton Generation by a Moderate-Intensity Ultrashort-Pulse Laser Interaction with H_2O Nanowire Targets

A. Zigler,[1] T. Palchan,[1] N. Bruner,[1] E. Schleifer,[1] S. Eisenmann,[1] M. Botton,[1] Z. Henis,[1] S. A. Pikuz,[2] A. Y. Faenov, Jr.,[2] D. Gordon,[3] and P. Sprangle[3]

[1]*Racah Institute of Physics, Hebrew University, Jerusalem 91904, Israel*
[2]*Joint Institute for High Temperatures, Russian Academy of Sciences, Moscow, Russia*
[3]*Plasma Physics Division, Naval Research Laboratory, Washington, D.C. 20375, USA*

(Received 26 December 2010; published 30 March 2011)

We report on the first generation of 5.5–7.5 MeV protons by a moderate-intensity short-pulse laser ($\sim 5 \times 10^{17}$ W/cm^2, 40 fsec) interacting with frozen H_2O nanometer-size structure droplets (snow nanowires) deposited on a sapphire substrate. In this setup, the laser intensity is locally enhanced by the snow nanowire, leading to high spatial gradients. Accordingly, the nanoplasma is subject to enhanced ponderomotive potential, and confined charge separation is obtained. Electrostatic fields of extremely high intensities are produced over the short scale length, and protons are accelerated to MeV-level energies.

DOI: 10.1103/PhysRevLett.106.134801 PACS numbers: 41.75.Jv, 52.35.Mw, 52.38.Kd, 52.59.−f

Compact sources of high-energy protons (50–200 MeV) are expected to be key technology in a wide range of scientific applications [1–8]. One promising approach is the target normal sheath acceleration (TNSA) scheme [9,10], holding a record level of 67 MeV protons generated by a petawatt laser [11]. More recently, a new regime, namely, the coherent acceleration of ions by lasers has emerged [12], promising an improved efficiency and higher energy of the ions. Illuminating diamondlike carbon ultrathin foil targets by (10^{19}–10^{20}) W/cm^2 lasers, 13 MeV protons and 71 MeV carbon ions were produced by a 1.2 J, 45 fsec laser [13], and 35 MeV protons and 185 MeV carbon ions by a 40 J, 700 fsec laser [14]. Nanoscale targets were also considered [15,16]. In general, laser intensity exceeding 10^{18} W/cm^2 is required to produce MeV-level protons. Enhancing the energy of generated protons using compact laser sources is a very attractive task nowadays. Previous studies of a target of nanometer-sized frozen water droplets (snow nanowires) [17,18] illuminated by a moderate energy level short-pulse laser have demonstrated a significantly improved absorption of the laser energy by the snow nanowire-deposited target compared to sapphire-only targets.

In this Letter, we report on the first generation of 5.5–7.5 MeV protons by a modest-energy laser. The protons are obtained from a snow nanowire target that is positioned at the focal point of a 0.5 TW, 40 fsec laser at the Hebrew University High Intensity Laser facility [see Fig. 1(a)]. The laser operates at a central wavelength of 798 nm and is focused by an off-axis parabolic mirror ($f/3.3$) to a spot area of 80 μm^2 (FWHM) on the target. The laser irradiates the snow nanowire interface at 60 deg to the normal. A prepulse of time duration of the same time scale as the main pulse originates in the regenerative preamplifier and precedes the main pulse by 10 nsec. The main pulse to prepulse contrast ratio is 10^3. A microscopic imaging system is used to make sure that the laser irradiates a fresh patch of snow nanowires at every shot. The diagnostics of the accelerated protons consist of CR39 solid-state nuclear track detector (SSNTD) plates, covered by various layers of B10 and aluminum foils serving as energy filters. The detector is positioned at a distance of 35 mm from the target's plane along the normal, collecting protons from a solid angle of 1.2 sr. A reference CR39 detector is placed at a position hidden from the target to measure the background signal. Each detector with energy filter setup is exposed to a series of 30–50 laser shots before being pulled out of the vacuum chamber and processed.

A typical scan of the processed CR39 detector is shown in Fig. 1(b). The proton tracks (bright, circular spots) are accumulated in bunches, with no preferred orientation on the detector plane. Proton bunches are accelerated into relatively small solid angles of about 1.6 μsr. We therefore deduce that a bunch represents several protons accelerated in one shot at the same direction. Considering the stopping power of the aluminum foil (of thickness 208 μm) that is placed in front of the CR39 detector, we conclude that the

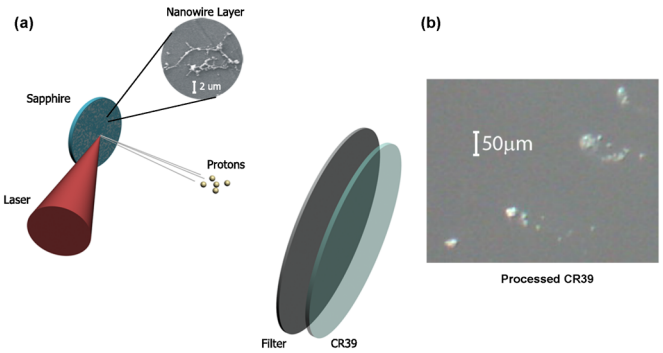

FIG. 1 (color online). (a) Schematics of experimental setup. (b) Proton track bunches on a processed CR39 plate.

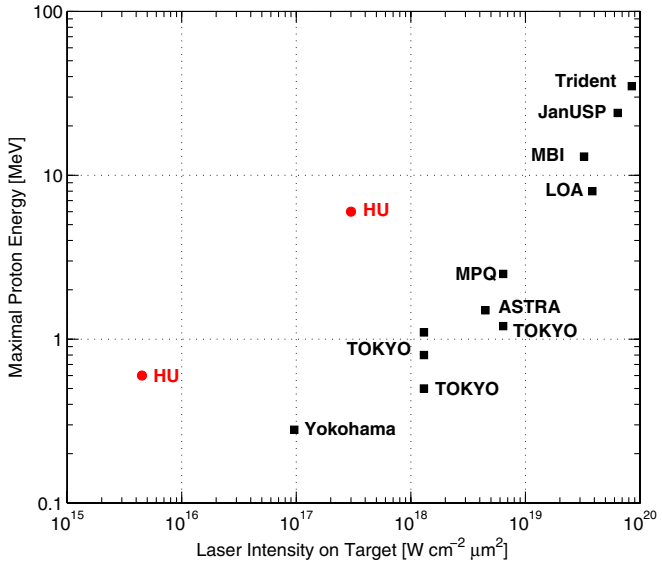

FIG. 2 (color online). Maximal proton energy in MeV versus the intensity for short (< 100 fsec) Ti:sapphire laser systems (data taken from Refs. [3,13,20–23]).

energy of the fastest protons is 5.5–7.5 MeV. The number of proton tracks behind the filters is 4708 ± 707 protons per shot per sr compared to a background level of 2942 ± 1079 on the unexposed CR39 detector. Note that the detector is placed at an angle to the laser beam, thus the protons are not accelerated along the laser direction as in the planar TNSA and diamondlike carbon experiments. The scaling of the proton's energy as a function of the intensity of the main pulse is shown in Fig. 2. The data obtained in the current experiments (marked HU in Fig. 2) follows the conventional relation $E_{\max} \propto (I\lambda^2)^{0.5}$ but is achieved with lower energy and intensity levels of the laser.

A possible explanation of the experimental results starts with the assumption that the arrangement of the nanowires on the target is amorphous due to the deposition method. Based on our previous analysis of the snow nanowire target [17,18] we estimate that the distance between adjacent nanowires (~ 5–10 μm) is large compared to their diameter (~ 0.1 μm) [see Fig. 1(a)]. Furthermore, the spot size of the laser beam is small enough so that it interacts with few nanowires. For simplicity, we assume that the laser (prepulse and main pulse) interacts with only one nanowire. The highly efficient absorption of the laser energy by the snow nanowire target [17] points to the fact that the prepulse vaporizes the nanowire (note that the plasma skin depth is larger than the width of the nanowire). The temperature of the formed plasma is estimated to be about 2–5 eV. During the 10 nsec interval between the prepulse and the main pulse, the plasma freely expands away from the nanowire forming a nanoplasma column (NPC). The main pulse therefore interacts with a nonuniform cylindrical symmetric plasma density (see Fig. 3), unlike the conventional TNSA foil configuration where the laser

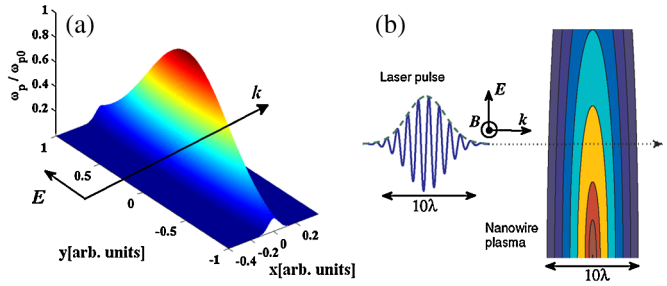

FIG. 3 (color online). (a) The plasma density as a function of planar distance from the original position of the nanowire ($x = 0, y = 0$). (b) The laser electric field E propagation through the nanoplasma at a direction k.

interacts with constant or planar plasma distribution. Note the important role of the prepulse in forming the NPC.

For brevity of presentation, the main laser pulse is assumed to propagate in a direction perpendicular to the NPC symmetry axis. Even with these simplifications the interaction is essentially three dimensional as the laser breaks the cylindrical symmetry of the NPC. The main-pulse length is larger than the width of the NPC. Accordingly, the averaged ponderomotive potential of the laser in the vicinity of the NPC can be calculated using the quasistatic approximation. We model the NPC as a prolate spheroid with conductivity and dielectric constant related to the plasma parameters. The main result of this model is the field enhancement near the NPC by an amount related to the NPC radius and the distance from it. To obtain a clear, yet representative, one-dimensional model of the acceleration process, we analyze the interaction of the laser with the plasma distributed along one ray in parallel to the laser wave vector. The density profile of the NPC along a ray and the enhancement factor of the laser amplitude are described in Fig. 4. We now solve a set of one-dimensional fluid equations for the electrons and ions in a plasma of the given distribution function assuming that the main pulse propagates from the left edge to the right and is subject to field enhancement. The effect of the ponderomotive potential in this case is enhanced by two factors. First is the local field enhancement which is translated to direct

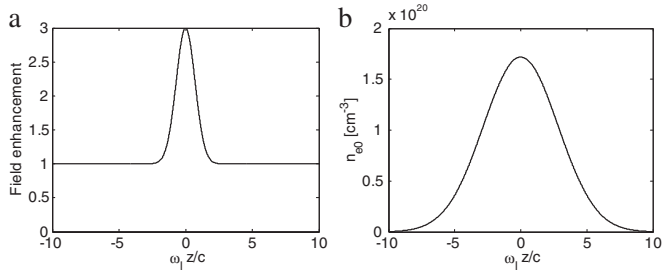

FIG. 4. (a) The localized field enhancement due to the NPC. (b) The initial plasma density.

enhancement of the amplitude. Next is the increment of the gradient of the ponderomotive potential due to the local character of the field enhancement. The plasma electrons are therefore subjected to a greatly increased force, and accordingly the density is modified to a greater extent than is expected of the laser intensity by itself. Figure 5 demonstrates this enhancement for six time frames. Solid lines show the electrons' density at a given time, broken lines are the initial density of the electrons (namely, the ions' density), and dotted lines represent the laser envelope. Note that as the laser pulse is near the NPC, its shape is strongly affected by the local field enhancement [Figs. 5(c) and 5(d)]. The electrons respond to the ponderomotive potential and the self-consistent electrostatic potential, and their density is changed as the pulse propagates through the plasma.

Figure 6 shows the distribution of the electrons (black line) after the passage of the laser pulse including the field enhancement. The exact position and magnitude of the electron cloud is a function of the maximal enhancement and gradient of the NPC. We note that the level to which the electrons are compressed depends also on the temperature they gain in the process. Up to this stage the ions are practically not affected by the laser pulse at all. However, they start to respond to the electrostatic potential of the electron cloud. Following the conventional model [19], we estimate the temperature of the electrons in the cloud, the scale length that determines the intensity of the accelerating field, and the accelerating distance. To estimate the temperature of the electrons we use the following expression:

$$kT_{\mathrm{hot}} \sim m_e c^2 \left[\sqrt{1 + \frac{a_{\mathrm{tip}}^2 I \lambda^2}{1.37 \times 10^{18}}} - 1 \right].$$

Here the conventional scaling of the laser intensity is multiplied by the field enhancement of the NPC, a_{tip} (squared for intensity). Taking this factor to be 10 (which means a modest field enhancement of $\sim$3), we find that the temperature of the hot electrons in the cloud is of the order of 200–300 keV. Next we estimate the scale length of the local plasma using the calculations of the cold fluid model. Based on the fluid model we find that the electron cloud is ramped up by a steep gradient which is estimated to be $(0.1\text{–}0.05)\lambda$ (see left-hand inset in Fig. 6). Furthermore, we estimate that the length over which the protons can be accelerated is approximately λ (see right-hand inset in Fig. 6). Combining the above we find that the protons can be accelerated to about $(10\text{–}20)kT_{\mathrm{hot}}$, which for laser intensity at the range of 4.5×10^{17} W/cm^2 is 2–6 MeV. Several remarks are in order. First, we would like to stress that the most energetic protons are accelerated in a direction that is defined by the orientation between the NPC and the wave vector of the laser. This is supported by our experimental results where we find bunches of accelerated protons and not a uniform distribution. Furthermore, as this acceleration scheme is ballistic in nature, we do not expect a large amount of protons to reach this energy unless specially designed targets are used. Finally, three-dimensional effects, which will not change the basics of the accelerating scheme, must be considered to describe the exact position of the electron cloud with respect to the NPC depending on the parameters of the NPC and the laser.

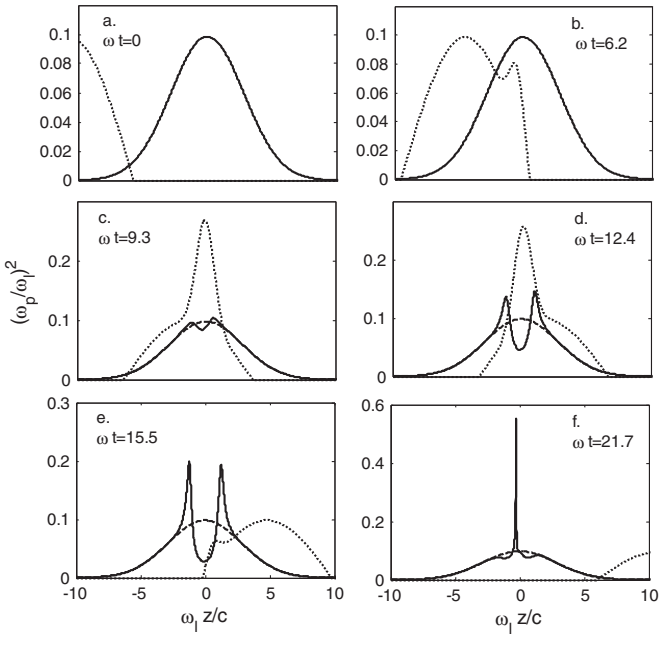

FIG. 5. The density of the electrons (solid line) at six time frames. The laser envelope (dotted line) is enhanced by the NPC. Broken lines show the initial distribution of the electrons.

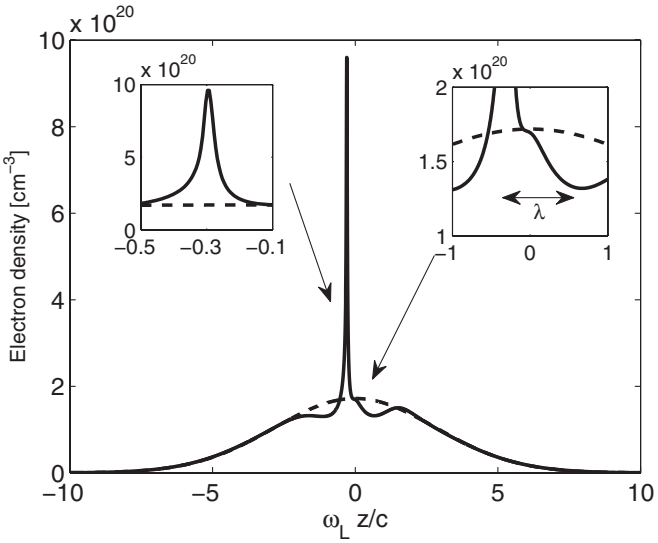

FIG. 6. Electron density normalized to the laser frequency before and after the main laser pulse has passed the frozen H_2O nanowire. Left-hand inset: Enlargement of the region of peak electron density. Right-hand inset: Enlargement of the ions' acceleration length.

In conclusion, we have experimentally demonstrated generation of 5.5–7.5 MeV protons from snow nanowire targets by modest, 4.5×10^{17} W/cm^2, laser intensities, which is an order of magnitude higher compared with previous experiments with such laser intensities. The protons are accelerated by the enhanced interaction of the laser field and the nanoplasma column generated by the prepulse near the tip of the nanowire. Engineered nanowire targets and prepulse intensity can improve the interaction scheme by increasing the number of accelerated protons and directing them in a predesigned direction.

[1] B. M. Hegelich *et al.*, Nature (London) **439**, 441 (2006).
[2] H. Schwoerer *et al.*, Nature (London) **439**, 445 (2006).
[3] J. Fuchs *et al.*, C.R. Physique **10**, 176 (2009).
[4] P. V. Nickles *et al.*, J. Opt. Soc. Am. B **25**, B155 (2008).
[5] G. Sarri *et al.*, New J. Phys. **12**, 045006 (2010).
[6] S. Fritzler *et al.*, Appl. Phys. Lett. **83**, 3039 (2003).
[7] M. Roth *et al.*, Phys. Rev. Lett. **86**, 436 (2001).
[8] K. Ledingham, Nature Phys. **2**, 11 (2006).
[9] S. Hatchett *et al.*, Phys. Plasmas **7**, 2076 (2000).
[10] S. C. Wilks *et al.*, Phys. Plasmas **8**, 542 (2001).
[11] S. A. Gaillard *et al.*, in *Proceedings of the APS 51st Annual Meeting of the Division of Plasma Physics* (APS, New York, 2009), Abstract No. G06.003.
[12] T. Tajima, D. Habs, and X. Yan, in *Reviews of Accelerator Science and Technology*, edited by A. W. Chao and W. Chou (World Scientific, Singapore, 2009), Vol. 2, pp. 201–228.
[13] S. Steinke *et al.*, Laser Part. Beams **28**, 215 (2010).
[14] A. Henig *et al.*, Phys. Rev. Lett. **103**, 045002 (2009).
[15] S. Bagchi *et al.*, Appl. Phys. B **88**, 167 (2007).
[16] B. Ramakrishna *et al.*, Phys. Plasmas **17**, 083113 (2010).
[17] T. Palchan *et al.*, Appl. Phys. Lett. **90**, 041501 (2007).
[18] T. Palchan *et al.*, Appl. Phys. Lett. **91**, 251501 (2007).
[19] S. C. Wilks and W. L. Kruer, IEEE J. Quantum Electron. **33**, 1954 (1997).
[20] T. Ceccotti *et al.*, Phys. Rev. Lett. **99**, 185002 (2007).
[21] L. A. Gizzi *et al.*, Nucl. Instrum. Methods Phys. Res., Sect. A **620**, 83 (2010).
[22] D. Neely *et al.*, Appl. Phys. Lett. **89**, 021502 (2006).
[23] M. Borghesi *et al.*, Fusion Sci. Technol. **49**, 412 (2006).